^{85,87}Rb, ^{14}N NMR Studies of Successive Phase Transitions and Incommensurate Phase in $R_2Pb[Cu(NO_2)_6]$ (R = NH_4, Rb)

Hiroyuki Ishikawa, Motohiro Mizuno, and Masahiko Suhara

Department of Chemistry, Faculty of Science, Kanazawa University, Kanazawa 920-1192 Japan

Reprint requests to Dr. M. M.; E-mail: mizuno@wriron1.s.kanazawa-u.ac.jp

Z. Naturforsch. **57 a,** 403–407 (2002); received January 23, 2002

Presented at the XVIth International Symposium on Nuclear Quadrupole Interactions, Hiroshima, Japan, September 9-14, 2001.

^{85,87}Rb and ^{14}N NMR spectra and spin-lattice relaxation time (T_1) were measured for $R_2Pb[Cu(NO_2)_6]$ (R = Rb, NH_4). The quadrupole coupling constant (e^2Qq/h), asymmetry parameter (η), and the effective transverce relaxation time (T_2^*) were estimated from the simulation of NMR spectra. The NMR spectra in commensurate phase III can be explained by the superposition of two components corresponding to two inequivalent sites of the R^+ ion. In the incommensurate phase II, e^2Qq/h and T_2^* decreased with increasing temperature, while η was almost temperature independent. T_1 in phase II is found to be determined by the contribution of acoustic phason with multi-soliton limits.

Key words: Phase Transition; Incommensurate Phase; ^{14}N NMR; ^{85,87}Rb NMR

Introduction

R_2Pb $[Cu(NO_2)_6]$ (R = Rb, NH_4; abbreviated as Rb-PCN and NH_4-PCN, respectively) are known to undergo successive phase transitions induced by the cooperative Jahn-Teller effect of $[Cu(NO_2)_6]^{4-}$ [1 - 5]. As the temperature is lowered, Rb-PCN transforms from the cubic phase I (space group Fm3) to the incommensurate phase II (Fmmm) at T_I = 313 K, and further into the commensurate phase III ($C\bar{1}$) at T_C = 274 K. In phase II, the modulation wave of the local Jahn-Teller distortion of $[Cu(NO_2)_6]^{4-}$ octahedra is directed to [110]. In phase III, two crystalographically inequivalent $[Cu(NO_2)_6]^{4-}$ octahedra, elongated along [100] and [010], exist. Similar phase transitions occur at T_C = 287 K and T_I = 316 K for NH_4-PCN [4].

Previously, ^{87}Rb NMR spin-lattice relaxation times T_1 in phase II, smaller than in phases I and III, and critical behavior of the ^{14}N NQR spin-lattice relaxation time T_{1Q} for the nitrogen in the -NO_2 group around T_C have been reported [3]. In this work, the ^{85,87}Rb and ^{14}N (I = 5/2, 3/2 and 1, respectively) NMR spectra and T_1 were measured in phases I, II, and III. We investigate the crystal dynamics and crystal structure of Rb-PCN and NH_4-PCN in each phase by analyzing ^{85,87}Rb and ^{14}N NMR spectra and T_1, which are dominated by the nuclear quadrupole interaction and the paramagnetic dipolar interaction. We also discuss the mechanism of nuclear relaxation in phase II due to the incommensurate modulation.

Experimental

The crystals of Rb-PCN and NH_4-PCN were grown from RNO_3 (R = Rb, NH_4), $NaNO_2$, $Pb(NO_3)_2$, and $Cu(NO_3)_2{\cdot}3H_2O$ in aqueous solution. We used powder samples for the NMR experiments. ^{85,87}Rb and ^{14}N NMR were measured using a CMX-300 spectrometer at 28.8, 97.7 and 21.6 MHz, respectively. The NMR spectra were measured by the quadrupole echo sequense ($(\pi/2)_x$-τ-$(\pi/2)_y$-τ-acq) for both ^{14}N and ^{85}Rb, and a single pulse for ^{87}Rb. The T_1 measurements were made by the inversion recovery method.

Results and Discussion

NMR Spectra

Figure 1 shows ^{14}N and ^{85,87}Rb NMR spectra in phases I, II, and III. In phase I, the spectra were struc-

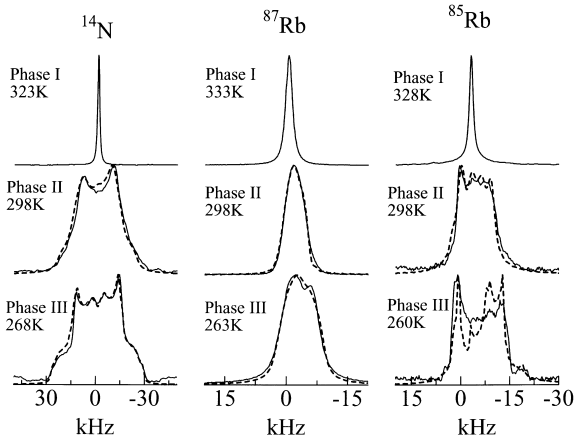

Fig. 1. ^{14}N and ^{85,87}Rb NMR spectra in each phase. The solid and broken lines show the observed and the theoretical spectra, respectively.

tureless. In phases II and III, to the lineshape of the ^{14}N NMR spectrum mainly contributed the first-order quadrupole interaction (ω_{Q1}) and the paramagnetic dipolar interaction (ω_{P}) between the resonant nuclei and the Cu^{2+} ions. ω_{Q1} and ω_{P} are written by the second-order Wigner rotation matrix [6 - 11] as

$$\omega_{\mathrm{Q1}} = \sqrt{\frac{3}{2}} \sum_{n,m=-2}^{2} D_{0n}^{(2)*}(\psi,\theta,\phi) D_{nm}^{(2)*}(\alpha,\beta,\gamma) T_{m\mathrm{Q}}^{(2)}, \tag{1}$$

$$T_{0\mathrm{Q}}^{(2)} = \sqrt{\frac{8}{3}} e^2 Qq/\hbar, T_{\pm 2\mathrm{Q}}^{(2)} = \frac{\eta}{4} e^2 Qq/\hbar, \tag{2}$$

$$\omega_{\mathrm{P}} = \sum_i \omega_{\mathrm{P}i}, \tag{3}$$

$$\omega_{\mathrm{P}i} = \sum_{n,m=-2}^{2} D_{0n}^{(2)*}(\psi,\theta,\phi) D_{n0}^{(2)*}(\alpha_i',\beta_i',\gamma_i') \omega_{Di}, \tag{4}$$

$$\omega_{\mathrm{D}i} = 2\pi\nu_{\mathrm{D}i}, \tag{5}$$

$$\nu_{\mathrm{D}i} = \nu_{\mathrm{Diso}} + \frac{1}{2}[\nu_{\mathrm{D}zz}(3\cos^2\beta_i'' - 1) + (\nu_{\mathrm{D}xx} - \nu_{\mathrm{D}yy})\sin^2\beta_i''\cos 2\gamma_i''], \tag{6}$$

where $\omega_{\mathrm{P}i}$ is the paramagnetic dipolar interaction between the resonant nuclei and i-th Cu^{2+} ion. (ψ,θ,ϕ), (α,β,γ) and $(\alpha_i',\beta_i',\gamma_i')$ represent the Euler angles for the transformation from the laboratory axes to the crystal axes, from the crystal axes to the principal axes system of the quadrupolar tensor and from the crystal axes to the principal axes system of the dipolar tensor between the resonant necleus and the i-th Cu^{2+} ion, respectively. β_i'' and γ_i'' are angles connecting the direction of the external field and the principal axes system of the **g**-tensor of i-th Cu^{2+} ion.

The lineshapes of the ^{85,87}Rb NMR spectra for the central transition are mainly dominated by the second-order quadrupole interaction(ω_{Q2}) and the paramagnetic dipolar interaction. ω_{Q2} is given by [12, 13]

$$\omega_{\mathrm{Q2}} = \frac{-4C_{\mathrm{Q}}^2}{\omega_{\mathrm{L}}} \left\{ I(I+1) - \frac{3}{4} \right\} \left\{ R_{2-2}^{\mathrm{Q}} R_{22}^{\mathrm{Q}} + 2R_{2-1}^{\mathrm{Q}} R_{21}^{\mathrm{Q}} \right\}, \tag{7}$$

$$C_{\mathrm{Q}} = \frac{e^2 Qq}{4I(2I-1)\hbar}. \tag{8}$$

Here, ω_{L} is the Larmor frequency and

$$R_{2m}^{\mathrm{Q}} = \sum_{n,n'=-2}^{2} D_{mn}^{(2)*}(\psi,\theta,\phi) D_{nn'}^{(2)*}(\alpha,\beta,\gamma) \rho_{2n'}^{\mathrm{Q}}, \tag{9}$$

where $\rho_{2n'}^{\mathrm{Q}}$ is the tensor element in the principal axis system [13]. The echo signal of ^{14}N NMR is written as [14]

$$G(t,\theta,\phi) = K\cos(\omega_{\mathrm{P}}\tau)\exp(i\omega_{\mathrm{P}}(\tau+t)) \cdot \cos(\omega_{\mathrm{Q1}}t)\exp(-T_2^{*-1}(2\tau+t)). \tag{10}$$

For the analysis of the ^{85,87}Rb NMR spectra,

$$G(t,\theta,\phi) = K\exp\left[(i(\omega_{Rb} - \omega_P) - T_2^{*-1})t\right] \tag{11}$$

was used. Here, T_2^* and K are the effective transverse relaxation time and a constant, respectively. The signal of the powder sample is given by

$$G(t) = \int_0^{2\pi}\int_0^{\pi} G(t,\theta,\phi)\sin\theta\,\mathrm{d}\theta\,\mathrm{d}\phi. \tag{12}$$

The NMR spectrum is obtained by the Fourier transform of $G(t)$.

ω_{P} was estimated from the crystal data [4, 2], and the contribution from Cu^{2+} ions with 7^3 primitive cells around the resonant nucleus was calculated. The

Table 1. e^2Qq/h and η, determined by the simulation of ^{85,87}Rb and ^{14}N NMR spectra.

Sample (observed nucleus)	Phase	e^2Qq/h (MHz)	η
$(NH_4)_2Pb[Cu(NO_2)_6]$(^{14}N)	II	26 - 32$\times10^{-3}$	0.2
	III	40 $\times$ 10^{-3}	0.09
		38 $\times$ 10^{-3}	0.6
$Rb_2Pb[Cu(NO_2)_6]$(^{85}Rb)	II	2.9 - 3.3	0.2
	III	3.55	0.09
		3.25	0.6
$Rb_2Pb[Cu(NO_2)_6]$(^{87}Rb)	II	1.30 - 1.45	0.2
	III	1.4	0.09
		1.3	0.6

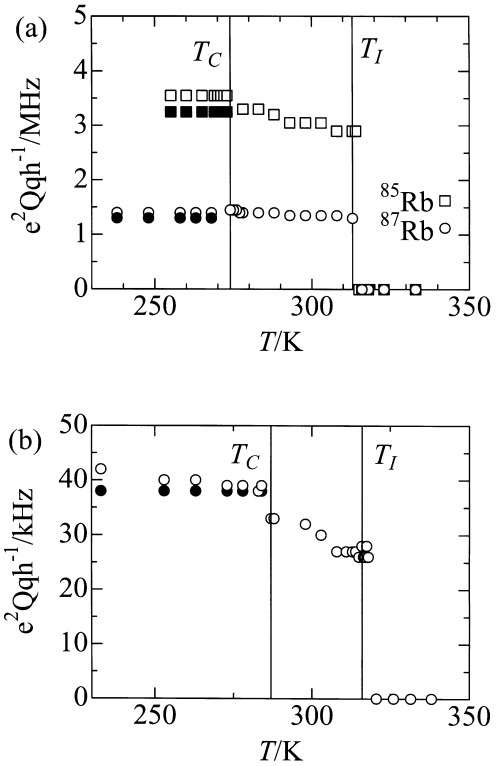

Fig. 2. Temperature dependence of e^2Qq/h determined by NMR spectral simulation. ^{85,87}Rb in Rb-PCN(a) and ^{14}N in NH_4-PCN(b). Open and closed symbols in phase III correspond to the components with η=0.09 and 0.6, respectively.

spectral simulation was performed using (1 - 12) with e^2Qq/h, η, T_2^*, α, β, and γ as parameters.

(α, β, γ) was obtained as (–0.8, 63, –59) for phases II and III from the spectral simulation. The temperature dependence of e^2Qq/h determined by the spectral simulation is shown in Figure 2. In

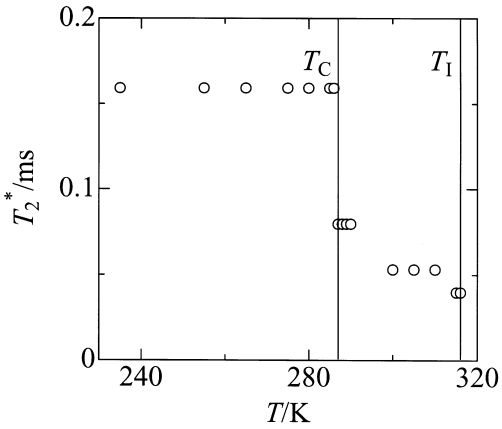

Fig. 3. Temperature dependence of T_2^* determined by ^{14}N NMR spectral simulation in NH_4-PCN.

phase II, e^2Qq/h increased with decreasing temperature, whereas η was almost constant (0.2). A sudden change in e^2Qq/h was observed at T_C. In phase III, the spectral lineshapes are explained by superposition of two spectra corresponding to inequivalent two sites of the R^+ ion [5]. e^2Qq/h and η in each phase are listed in Table 1. T_2^*, estimated by ^{14}N NMR spectral simulation is shown in Figure 3. In phase II, T_2^* is shorter than in phase III, and increased with decreasing temperature. We consider that the shorter T_2^* in phase II is caused by the modulation wave. T_2^*, which decreased with increasing temperature would indicate the soliton broadening [15].

Spin-lattice Relaxation Time T_1

Figure 4 shows the temperature dependences of ^{85,87}Rb and ^{14}N NMR T_1 in Rb-PCN and NH_4-PCN, respectively. T_1 shows discontinuous jumps at the transition points T_I and T_C. The temperature dependence of ^{85,87}Rb T_1 of Rb-PCN in phase I can be explained by the paramagnetic dipolar interaction between the resonant nuclei and Cu^{2+} ion. Then the relaxation rate T_{1P}^{-1} is written as [8, 16],

$$T_{1P}^{-1} = \frac{2}{15}\gamma^2 g^2 \mu_B^2 \cdot \sum_i r_i^{-6} S(S+1)\left\{\frac{3\tau_e}{1+\omega_L^2\tau_e^2} + \frac{7\tau_e}{1+\omega_e^2\tau_e^2}\right\}, \quad (13)$$

where γ is the gyromagnetic ratio of the resonant nucleus, μ_B the Bohr magneton, g the isotropic g-value

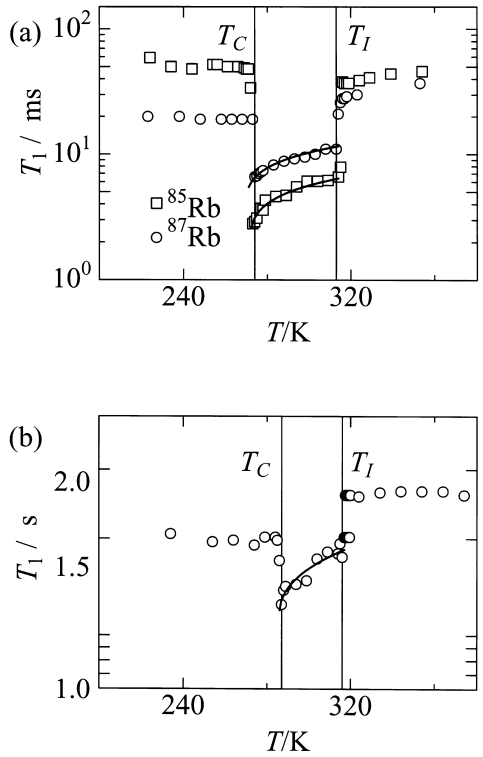

Fig. 4. Temperature dependence of NMR T_1 for ^{85,87}Rb in Rb-PCN(a) and ^{14}N in NH_4-PCN(b). The solid lines show the theoretical curves of eq. (20) as described in the text.

for Cu^{2+}, ω_L the angular NMR frequency, ω_e the ESR angular frequency, and τ_e the correlation time of the electron spin. r_i is the distance between the resonant nucleus and i-th Cu^{2+} ion. In the 7.0 T magnetic field, $\omega_L \ll \tau_e \ll \omega_e$ can be assumed, and (13) can be simplified as

$$T_{1P}^{-1} = \frac{2}{15}\gamma^2 g^2 \mu_B^2 \sum_i r_i^{-6} S(S+1) 3\tau_e. \quad (14)$$

When τ_e is dominated by the thermal jump between different Jahn-Teller distortions, τ_e can be written as

$$\tau_e = \tau_0 \exp(\Delta/kT), \quad (15)$$

where Δ is the activation energy for the jump between the different Jahn-Teller configurations. The Δ value and the pre-exponential factor τ_0 were obtained as $440 \pm 50\,\mathrm{cm}^{-1}$ and $(1.0 \pm 0.2) \times 10^{-11}$ s, respectively, from ^{85,87}Rb NMR T_1. The temperature independent ^{85,87}Rb T_1 in phase III and ^{14}N T_1 in phases I and III are considered to be dominated by the exchange interaction between Cu^{2+} ions.

^{85,87}Rb and ^{14}N T_1 in phase II are shorter than those in phases I and III. These results indicate that the relaxations of ^{85,87}Rb and ^{14}N in the incommensurate phase are dominated by the dynamics of the modulation wave. T_1 in the incommensurate phase is represented by the sum of contributions from amplitudon and phason given by T_{1A} and $T_{1\varphi}$, respectively, as [15, 17]

$$T_1^{-1} = T_{1A}^{-1} + T_{1\varphi}^{-1}. \quad (16)$$

The amplitudon has a typical soft mode behaviour with the approaching T_I and T_{1A} is described by [15, 17]

$$T_{1A}^{-1} \propto (T_I - T)^{-1/2}. \quad (17)$$

Therefore T_1 of ^{14}N and ^{85,87}Rb in the incommensurate phase are considered to be mainly determined by the phason.

The phason behaviour can be discussed by the plane wave limit and the multi-soliton limit models separately. In the plane wave limit, the relaxation rate $T_{1\varphi}^{-1}$ is represented as [18, 19]

$$T_{1\varphi}^{-1} \propto T(\sqrt{1 + (\omega_L/\omega_\varphi)} + 1)^{-1/2}, \quad (18)$$

where ω_φ is the phason gap frequency. On the other hand, in the multi-soliton limit, the phason branch consists of two parts. One is the acoustic branch corresponding to phase oscillations of the incommensurate multi-soliton lattice, and the other is the optical branch corresponding to phase oscillation of the commensurate regions. In this situation, $T_{1\varphi}^{-1}$ can be written as

$$T_{1\varphi}^{-1} = (T_{1\varphi})_{ac}^{-1} + (T_{1\varphi})_{op}^{-1}, \quad (19)$$

where $(T_{1\varphi})_{ac}^{-1}$ and $(T_{1\varphi})_{op}^{-1}$ are the contributions from the acoustic and optical parts, respectively. The contribution of $(T_{1\varphi})_{op}^{-1}$ doesn't have a critical temperature dependence [15]. $(T_{1\varphi})_{ac}^{-1}$ is approximately evaluated from the dispersion relation which describes the acoustic phason branch in the multi-soliton lattice [15]. In the region of $\omega_\varphi \ll \omega_L$, $(T_{1\varphi})_{ac}^{-1}$ is written as

$$(T_{1\varphi})_{ac}^{-1} \propto \{\omega_L(T - T_C)\}^{-1/2}. \quad (20)$$

In the region of $\omega_L \ll \omega_\varphi$, $(T_{1\varphi})^{-1}_{\rm ac}$ has no longer the $\omega_{\rm L}$ dependence and can be represented as

$$(T_{1\varphi})^{-1}_{\rm ac} \propto (1 - T_{\rm C}/T)^{1/2} \quad (21)$$

by assuming the Landau theory for the temperature dependence of the inter-soliton distance [15].

In incommensurate phase II, T_1 of ^{85,87}Rb and ^{14}N decreased with decreasing temperature, and showed critical behaviour around $T_{\rm C}$. These results suggest that the relations of ^{85,87}Rb and ^{14}N nuclei are dominated by the contribution of acoustic phasons in the region $\omega_\varphi \ll \omega_{\rm L}$. The solid lines in Fig. 4 show the theoretical fitting of (20) to the observed T_1. $T_{\rm C} \approx$ 270 and 285 K were obtained from the NMR T_1 in Rb-PCN and NH_4-PCN, respectively. The obtained $T_{\rm C}$ are lower than the reported $T_{\rm C}$ [3 - 5]. These discrepancies were reported for Raman scattering measurments in Rb_2ZnCl_4 and Rb_2ZnBr_4[20] and ^{133}Cs NMR in Cs_2HgCl_4 [19].

Conclusions

The temperature dependences of e^2Qq/h were estimated by the simulation of ^{14}N and ^{85,87}Rb NMR spectra. In phase II, e^2Qq/h increased with decreasing temperature. ^{85,87}Rb and ^{14}N NMR T_1 were dominated by the contribution of acoustic phasons at $\omega_\varphi \ll \omega_{\rm L}$. $T_{\rm C} \approx$ 270 and 285 K in Rb-PCN and NH_4-PCN, respectively, were determined as the phason softening temperatures. Two components were shown in the ^{14}N and ^{85,87}Rb NMR spectra of phase III, corresponding to two inequivalent sites of the R^+ ion. The increase in the ^{14}N NMR T_2^* with increasing temperature in phase II can be explained by the soliton broadening.

[1] T. Asaji, L. S. Prabhumirashi, and D. Nakamura, Z. Naturforsch. **41a**, 1154 (1986).
[2] S. Takagi and M. D. Joesten, Acta. Cryst. **B32**, 1278 (1976).
[3] M. Mizuno, M. Suhara, T. Asaji, and Y. Furukawa, Z. Naturforsch. **51a**, 721 (1996).
[4] T. Asaji, R. Ikeda, and D. Nakamura, Z. Naturforsch. **34b**, 1722 (1979).
[5] Y. Noda, M. Mori, and Y. Yamada, J. Phys. Soc. Japan **45**, 954 (1978).
[6] S. E. Woehler, R. J. Wittebort, S. M. Oh, D. N. Hendrickson, D. Inniss, and C. E. Stvouse, J. Amer. Chem. Soc. **108**, 2938 (1986).
[7] S. Ganapathy, P. R. Rajamaohanan, P. Ganguly, T. N. Venkatraman, and A. Kumar, J. Phys. Chem. A **104**, 2007 (2000).
[8] T. Iijima, K. Orii, M. Mizuno, and M. Suhara, Z. Naturforsch. **53a**, 447 (1998).
[9] R. R. Vold, in Nuclear Magnetic Resonance Probes of Molecular Dynamics, ed. by R. Tycko, Kluwer Academic Publishers, 1994, p. 27.
[10] M. S. Greenfield, A. D. Ronemus, R. L. Vold, R. R. Vold, P. D. Ellis, and T. E. Raidy, J. Magn. Reson. **72**, 89 (1987).
[11] M. E. Rose, in Elementary Theory of Angular Momentum; Wiley, New York 1957.
[12] K. Narita, J. Umeda, and H. Kusumoto, J. Chem. Phys. **44**, 2719 (1966).
[13] A. Medek and L. Frydman, J. Magn. Reson. **138**, 298 (1999).
[14] D. J. Siminovitch, M. Rance, K. R. Jeffrey, and M. F. Brown, J. Magn. Reson. **58**, 62 (1984).
[15] R. Blinc, Physics Reports **79**, 331 (1981).
[16] M. Mizuno, T. Asaji, D. Nakamura, and K. Horiuchi, Z. Naturforsch. **45a**, 527 (1990).
[17] R. Blinc and A. P. Levanyuk, Incommensurate Phases in Dielectrics 1. Fundamentals.
[18] P. Mischo, F. Decker, U. Häcker, K. P. Holzer, and J. Petersson, Phys. Rev. Lett. **78**, 2152 (1997).
[19] K. Suzuki, S. Ishimaru, and R. Ikeda, J. Phys. Soc. Japan **69**, 729 (2000).
[20] M. Quilichini, J. P. Mathieu, M. Le Postollec, and N. Toupry, J. Phys. (France) **43**, 787 (1982).